Majeed, S.; Fierro, D.; Buhr, K.; Wind, J.; Du, B.;
Boschetti de Fierro, A.; Abetz, V.:

Multi-walled carbon nanotubes (MWCNTs) mixed polyacrylonitrile (PAN) ultrafiltration membranes

In: Journal of Membrane Science (2012) Elsevier

DOI: 10.1016/j.memsci.2012.02.029

Multi-walled Carbon Nanotubes (MWCNTs) Mixed Polyacrylonitrile (PAN) Ultrafiltration Membranes

Shahid Majeed, Daniel Fierro,[§] Kristian Buhr, Jan Wind, Bing Du, Adriana Boschetti-de-Fierro,[#] Volker Abetz[*]

Institute of Polymer Research, Helmholtz-Zentrum Geesthacht, Max-Planck-Str. 1, 21502 Geesthacht, Germany.

§ Current address: School of Engineering, Reutlingen University, Alteburgstrasse 150, 72762 Reutlingen, Germany.

Current address: Gambro Dialysatoren GmbH, Research and Development, Holger-Crafoord-Str. 26, 72379 Hechingen, Germany.

[*] Corresponding author, e-mail: volker.abetz@hzg.de

Abstract

Hydroxyl functionalized multi-walled carbon nanotubes (MWCNTs) were blended with Polyacrylonitrile (PAN) to prepare ultrafiltration membranes by a phase inversion process. Three different concentrations of MWCNTs were used in PAN, i.e. 0.5, 1 and 2 wt%. The water flux of the membranes increased by 63% at 0.5 wt% loading of MWCNTs compared to neat PAN membranes. The water flux decreased upon further increase in the concentration of MWCNTs, but at 2 wt% loading it was still higher compared to pure PAN membranes. The surface hydrophilicity of the membranes was enhanced upon the addition of MWCNTs, as observed by contact angle measurements. The increased hydrophilicity might have an impact on the improved water flux. All the membranes showed a molecular weight cut off (MWCO) of

approximately 50 Kg/mol. Surface pore size analysis by scanning electron microscopy (SEM) showed no significant difference in the mean pore size of the nanocomposite membranes compared to the neat membranes. The cross section morphology was influenced by the introduction of MWCNTs where less but enlarged macrovoids were observed, particularly prominent at a loading of 2 wt% MWCNTs. The membranes containing 2wt% MWCNTs showed 36% improvement in resistance against compaction compared to neat membranes. Furthermore, the tensile strength of the membranes at 2wt% MWCNTs loading increased over 97% compared to neat ones.

Keywords: Ultrafiltration, mixed matrix membranes, carbon nanotube mixed membranes, membrane compaction.

1. Introduction

Membranes have proven themselves as promising separation candidates due to advantages offered by their high stability, efficiency, low energy requirement and ease of operation. Membranes with good thermal and mechanical stability combined with good solvent resistance are important for industrial processes. The growing interest in this area led to development of inorganic and polymeric membranes. Generally, inorganic membranes can provide the desired material properties for different separation processes. However, their performance and higher cost compared to polymeric membranes may become a hurdle in industrial applications.[1]

Polymer membranes are either porous or dense. Porous membranes are prepared mainly by a phase inversion process.[2] They often show a reduction of the permeate flux at higher pressure. This decrease in permeate flux may result from the

compaction of the originally porous structure to a more dense structure.[3] Tarnawski reported the compaction of a GR60P ultrafiltration membrane (MWCO 25,000 D). They found a non linear relationship between processing pressure and water flux for a pressure range varying from 0.8 to 30 bar. The compaction was considered to be the main reason for this behaviour.[4] Persson et al studied the compaction of Polysulfone (PS) and Cellulose acetate (CA) membranes. They pointed out that PS membranes undergo compaction because of their high porosity and more macrovoidic structures compared to CA membranes which have less porosity.[5]

A promising way to improve mechanical stability and separation performance of the porous membranes is the utilization of nanofillers.[3, 6-8] Addition of the fillers improves the mechanical stability and resistance against compaction as observed by Ebert *et al*. They prepared PVDF/TiO_2 blend membranes and tested them at a pressure of 30 bar. PVDF/TiO_2 membranes were clearly less susceptible to compaction compared to pure PVDF membranes.[3]

Carbon nanotubes (CNTs) are also appealing membrane fillers and act as extraordinary mass transport channels as studied by various research groups.[9-20] Choi et al. blended carboxylated multi-walled carbon nanotubes (MWCNTs) with polysulfone and prepared the membranes by phase inversion process.[21] The pure water flux increased by increasing MWCNTs content up to 1.5 wt% and then decreased with further loading of MWCNTs. The higher flux was attributed to a hydrophilic surface and large surface pores, resulting from the addition of MWCNTs. Tang *et al.* used PEG6000 and MWCNTs for the fabrication of chitosan porous membranes.[8] They observed that membranes with 10 wt% MWCNTs loading showed 4.6 times higher water flux than pure chitosan membranes. The higher water flux was

observed due to the formation of MWCNTs nanochannels in chitosan pores. Moreover, the tensile strength of the membranes increased with MWCNTs addition.

Polyacrylonitrile (PAN) micro and ultrafiltration membranes are widely used for water treatment as well as for recycling of industrial waste water e.g., in the pulp and paper industry. Kharul *et al.* reported an increase in transport properties of PAN ultrafiltration membranes by inorganic and organic base treatment.[22] Huang *et al.* observed an improvement of PAN membrane properties using Fe_3O_4 fillers.[23] In the present study, hydroxyl functionalized MWCNTs were used as fillers in PAN ultrafiltration membranes to improve the membrane transport properties and their mechanical stability. The membrane morphology was studied by SEM analysis while the dispersion of MWCNTs was investigated by TEM. The influence of different loadings of MWCNTs on water flux, separation performance and mechanical strength was studied. Additionally, the water flux at different feed pressures was measured to evaluate the membrane compaction which is a significant feature of this study.

2. Experimental

2.1 Materials

Polyacrylonitrile (PAN) having an averaged molecular weight of 200,000 g/mol was used in this study. *N*,*N*-dimethylformamide (DMF) was purchased from Merck. Hydroxyl functionalized MWCNTs having an average length of 15-20 μm were received from FutureCarbon®. Dextrans of different molecular weight were purchased from Serva Germany. All materials were used as received.

2.2 Membrane preparation

The casting solution for pure membranes comprised of 14 wt% PAN and 86 wt% DMF. MWCNTs, used in PAN nanocomposite membranes, contained 0.77

mmol/g hydroxyl functional groups. The solution for nanocomposite membranes contained 14 wt% PAN/MWCNTs and 86 wt% of DMF. The ratios between PAN and MWCNTs were kept as 99.5:0.5, 99:1 and 98:2, in order to maintain the loading of MWCNTs as 0.5, 1.0 and 2.0 wt%, respectively. PAN nanocomposite membranes were named as PAN0.5, PAN1 and PAN2 with respect to MWCNTs loading. For the preparation of the solution, MWCNTs were mixed with DMF and the resultant mixture was subjected to tip sonication (operated at 55 W) for 5 minutes. Then PAN was added to the dispersion and the mixture was stirred for 48 hours at 70°C to obtain a homogeneous solution. After cooling the solution to room temperature, it was degassed to ensure complete removal of air bubbles before membrane casting.

Non-woven polyester was attached to a glass plate and the polymer solution was cast with a doctor blade using a knife gap of 200 μm and followed by immediate immersion into the coagulation bath containing water at 20°C. After complete precipitation, the membranes were kept in water at room temperature for at least 24 hours to remove the remaining solvent prior to further characterization.

2.3 Membrane characterization

2.3.1 Fourier transform infrared spectroscopy (FTIR)

Fourier transform infrared (FTIR) spectroscopy was conducted using a Bruker Equinox 55. The samples were prepared by dispersing MWCNTs and the resultant membranes in KBr and pressing the mixed powders to form pellets. A KBr pellet was also prepared and used as a reference. The pellets were vacuum dried at 35 °C for 12 hours. The transmission measurements were carried out in a spectral range of 400-4000 cm^{-1} with a spectral resolution of 4 $cm^{-1}$and 64 scans.

2.3.2 Raman spectroscopy

The Raman spectra of PAN nanocomposite membranes and MWCNTs were measured by Bruker SENTERRA Raman microscope (λ = 785 nm, 10 mW) at room temperature.

2.3.3 Viscosity measurements

The viscosity of pure and nanocomposite PAN solutions was measured with a Europhysics® Rheo 2000 rheometer. Measurements were performed at constant shear rate of 100 s^{-1} for two minutes at 20 °C using cone/plate geometry (C25-1).

2.3.4 Scanning electron microscopy (SEM)

Scanning electron microscope studies on the membranes were carried out with a LEO Gemini 1550 VP from Zeiss with field emission cathode operated at 1 – 1.5 kV. The sample preparation for cross section analysis was done under cryogenic conditions. The membrane samples were sputtered by a very thin layer of Au/Pd.

2.3.5 Transmission electron microscopy (TEM)

For TEM studies, PAN nanocomposite membranes were fabricated by phase inversion on a glass plate without using non-woven polyester. Films having an approximate thickness of 50 µm were embedded with epoxy. Ultrathin sections of approximately 70 nm were cut in a Leica Ultra microtome under cryogenic conditions (-130°C). TEM experiments were carried out using FEI Tecnai G^2 F20 at 200kV in the bright field mode.

2.3.6 Porosity measurements

The porosity measurements of PAN membranes were carried out by dry-wet method using the expression given in equation 1:

$$Porosity = \frac{W_2 - W_1}{V \cdot d_{\text{butanol}}} \times 100\% \quad (1)$$

where w_1(g) is the weight of dry membrane, w_2(g) is the weight of membrane after dipping into 1-butanol for 2 hours, v (cm^3) is the volume of the membrane and $d_{butanol}$ (g/cm^3) is the density of 1-butanol at room temperature.

2.3.7 Contact angle measurements

The contact angle goniometer from Kruess was used to characterize the membrane surface polarity. The contact angle measurments on the membrane surface were carried out using a droplet of 5 µL at room temperature. As the final data, the mean of five values of contact angles on different areas of the membranes was used.

2.3.8 Water flux measurements

Water flux measurements were performed using a cross flow cell where the membranes with an effective area of 1.54 cm^2 were analyzed at 22°C. The schematic diagram of the cross flow cell is shown in Figure 1. The water flux was calculated by equation 2:

$$J = \frac{V}{S \cdot t} \quad (2)$$

where J represents the flux of the membrane measured as $lm^{-2}h^{-1}$, V the permeate volume measured in litre (l), S the membrane active surface area (m^2) and t the time required to obtain the required volume across the membrane (h).

The feed flow rate was kept at 480 ml/min and the flux was calculated at different transmembrane pressures i.e. 2, 4, 6, 8, and 10 bar in order to study the membrane compaction behaviour. For the flux measurements, the transmembrane pressure was maintained at 2 bar for 40 minutes and then water flux was calculated. Afterwards, the pressure was increased gradually and each pressure (4 to 10 bar) was maintained for 10 minutes followed by the measurement of water flux at that corresponding pressure. Three membrane stamps were analyzed to demonstrate the water flux behaviour.

2.3.9 Rejection measurements

330 ppm solution of dextrans with different molecular weights (Table 1) was prepared in deionized water. The membrane stamps having an effective area of 15.2 cm^2 were used and measurements were done in a Millipore cell under a pressure drop of 2 bar. The analysis of feed, permeate and retentate solutions was carried out by high performance liquid chromatography (HPLC) using a Waters® instrument equipped with a PSS® column (0.8 × 300 mm, 10 μm, Suprema Linear M) attached with a differential refractometer (Waters® 2410 RI), autosampler Waterss717+ at a flow rate of 1 ml/min at 35°C using tetrahydrofuran (THF) as internal standard. The results were calibrated with dextran standards. The values of retention were calculated using equation 3:

$$R = 1 - \frac{c_P}{(c_F + c_R)/2} \qquad (3)$$

Where c_P, c_F and c_R are the concentrations of permeate feed and retentate solutions (g/l), respectively.

2.3.10 Mechanical characterization

PAN nanocomposite membranes were prepared by phase inversion process without using non-woven polyester to carry out mechanical characterization. A universal testing machine from Zwick, model Z020, with a load cell of 20 N was used to carryout the analysis. 5 cm effective length and 1 cm width stripes of the membranes were measured at crosshead speed of 5 mm/min.

3. Results and discussion

3.1 Spectroscopic analysis

Figure 2 depicts the FTIR absorption spectra of MWCNTs and nanocomposite membranes. MWCNTs show the O-H stretching vibration at 3440 cm^{-1} and a conjugation of C=O with C=C bonds at 1630 cm^{-1}. A very small peak at 1735 cm^{-1} indicates the presence of carboxyl groups. Pure PAN membranes showed the typical nitrile (C≡N) peak at 2245 cm^{-1}, C-H stretching at 2933 cm^{-1} and deformation at 1452 cm^{-1}, respectively. These PAN peaks were also observed in PAN nanocomposite membrane (PAN2). The appearance of a hump at 3440 cm^{-1} in the PAN2 membrane can be related to OH groups present on MWCNTs. Marie *et al.* observed the hydrogen bond interaction between nitrile and hydroxyl functional groups by a shift of nitrile peak.[24] However, only a very slight shift (1.5 cm^{-1}) of the nitrile peak was observed in the nanocomposite membrane (PAN2), which is negligible to prove the hydrogen bonding between OH and C≡N groups (inset of Figure 2). OH functional groups present on MWCNTs are very less compared to the nitrile groups in the nanocomposite membranes which might be the reason of the negligible peak shift. In order to clarify the question of specific interactions between polymer matrix and MWCNTs, further investigation was made by Raman spectroscopy. Peak shifts were observed for PAN1 and PAN2 nanocomposite membranes in the tangential vibration mode (Figure 3). Both G (1601.26 cm^{-1}) and D (1306.76 cm^{-1}) bands of MWCNTs

were shifted ~8 cm^{-1} for PAN1 and PAN2 compared to MWCNTs. Similar shifts were also observed by Baskaran *et al.* in nanocomposites of MWCNTs and polybutadiene.[25] The coverage of MWCNTs surface with polymer chains is enhanced at low loadings of MWCNTs. This affects the movement of C-C bonds in the graphene plane due to CH-π interactions between the carbon atoms of the MWCNTs and the CH-groups of the polymer. Therefore, the observed peak shifts can be related to the CH- π interaction between PAN and MWCNTs.

3.2 Viscosity measurements

The rheological properties of PAN nanocomposite solutions were studied at 20°C and a constant shear rate of 100 s^{-1}. An increase in solution viscosity was observed with the addition of hydroxyl functionalized MWCNTs (Figure 4). A maximum value of the solution viscosity was observed with the highest loading of MWCNTs i.e 2wt%. The increase in viscosity with MWCNTs addition indicates the occurrence of good interaction between MWCNTs and the polymer.[26] Khatua *et al.* found out that the addition of clay nanoparticles to polymer blends reduced the domain size of polymer blends.[27] They reported that the viscosity of the polymer blends increases with nanoparticles where nanoparticles act as physical barrier that slows down the coalescence of dispersed domains. An increase in the viscosities of the polymer solutions with MWCNTs addition was observed by Choi *et al.* and Tang *et al*.[8, 21] The increase in viscosity with MWCNTs loading was related to the formation of a stronger network of polymer and MWCNTs rather than a MWCNTs-MWCNTs network. This result indicates strong MWCNT-polymer interactions. The viscosity of the polymer solution plays an important role to the morphology of the membranes prepared by a phase inversion process. Higher solution viscosities lead to a slower diffusion between the phase inversion components because of delayed exchange

between solvent and non solvent.[21,28] The increase in viscosities of PAN solution with MWCNTs led to nanocomposite membranes with reduced bulk porosities (Table 2). This can be explained by the delayed exchange between solvent and non solvent during the membrane formation. The impact of solution viscosities on the structures of the membrane surface and cross-section is discussed in the next section.

3.3 Microscopic characterization

The surface and cross sectional morphologies of the PAN membranes are shown in Figures 5 and 6, respectively. Identification of the surface pores is difficult due to irregular structure characteristics of the PAN membranes (Figure 5). The average pore size was determined by measuring the diameter of a minimum of 150 pores from three different scanning electron micrographs with 100k magnification. The surface morphology was not significantly affected by the addition of MWCNTs in terms of pore sizes and pore size density. The average pore sizes calculated from the SEM pictures are shown in Table 2, where the lack of influence of the nanofillers on the surface pore size is evident.

On the contrary, the cross sectional morphology (Figure 6) was greatly influenced by the addition of MWCNTs. The number of macrovoids decreased with MWCNTs loading and in PAN2 least macrovoids were observed. However, the size of the macrovoids was observed to increase with the content of MWCNTs. In PAN nanocomposite membranes, the enlarged macrovoids may result from the fusion of disappearing macrovoids as the solution viscosity increases. Celik *et al.* observed the reduction of macrovoids in polyethersulfone membranes upon addition of MWCNTs.[9] They related this effect with the increase in viscosity of casting solutions where increased viscosities slow down the phase separation. An increase in the size of the macrovoids might create the possibility of less number of pores with big pore size in

the cross-section of the membrane. The thickness of the thin separating layer on the top tends to increase with MWCNTs addition. SEM cross sectional pictures do not give any information about the dispersion state of MWCNTs. It is difficult to distinguish MWCNTs from cross sectional microstructures of the polymer (see for example a magnified area in Figure 6e). Therefore, TEM was used to study the dispersion of MWCNTs in PAN membranes (Figure 7a). In Figure 7b the MWCNTs are colored red to highlight them. From this TEM image it is evident that there exist small bundles of MWCNTs along with individual MWCNTs. The dispersion of individualised MWCNTs in some areas was quite homogenous but there were also some parts where also relatively bigger aggregates of MWCNTs were observed compared to the aggregates shown in Figure 7a. However, there were no areas without MWCNTs on the length scale of Figure 7a. Addition of MWCNTs in PAN gave rise to the membranes with improved hydrophilicity and tensile properties which are described in the next sections.

3.4 Contact angle measurements

The surface hydrophilicity of the membranes was influenced by the addition of hydrophilic MWCNTs containing hydroxyl functional groups. Figure 8 shows the decrease in contact angle with increasing amount of MWCNTs. The pure PAN membrane presents a hydrophilic surface in the absence of MWCNTs. However, a further increase in hydrophilicity of the membrane surface can be observed by MWCNTs addition. The increase in hydrophilicity with the addition of carboxyl functionalized MWCNTs was observed by Choi *et al* for polysulfone blend membranes and it played an important role in water permeation of the resultant membranes.[21]

3.5 Membrane permeation characterization

The water fluxes of pure and nanocomposite PAN membranes were measured at 2 bar transmembrane pressure. The influence of MWCNTs on the water flux of the membranes is shown in Figure 9. The error bar results from a minimum of three membrane stamps. The water flux increased by 63% at a loading of 0.5 wt% compared to neat membranes. The flux decreased for membranes with loadings of MWCNTs above 0.5 wt%. For PAN2 membranes, the flux was still 28% higher compared to the pure PAN membrane. The increased flux is usually attributed to increased surface pore sizes. However, SEM analysis revealed that there is no significant difference in the size of surface pores (Figure 5). A possible explanation for the increase in water flux values is the increase of hydrophilicity of the membrane surface by the addition of MWCNTs (Figure 8). As the water flux is largest for the nanocomposite membrane with 0.5 wt% of MWCNTs, the influence of hydrophilicity is compensated to some extent by the increase of the thickness of the dense top layer in membranes with higher MWCNT loadings.

Figure 9 also illustrates the separation performance of the membranes. 330 ppm solution of a mixture of dextrans (Table 1) was used for retention measurements. From the analysis of feed, permeate, and retentate, a separation curve was obtained applying equation 2. From the separation curve, the retentions at 6 Kg/mol and 50 Kg/mol are discussed in Figure 9. PAN0.5 rejected 47% of 6 Kg/mol dextran, which is lower compared to PAN0 (57%), PAN1 (57%) and PAN2 (56%). As the nanocomposite membranes did not present a significant difference in surface pore size and density when compared to the neat membranes, the rejection behaviour in the nanocomposite membranes might be explained by a combination of two opposite

effects. First, the increment in hydrophilicity enhances the permeation of water through the membrane. This affects the rejection positively by increasing the total amount of water molecules that permeates through the membrane without enhancing the permeability of dextran. Second, the higher water flux could affect negatively the retention values due to dragging of the solute[29] (dextran) which might happen in PAN0.5 where the least retention of dextran at 6 Kg/mol was observed. The low rejection of PAN0.5 might result from slightly larger pores or more interconnected pores compared to PAN0, PAN1, and PAN2. Hence, increased water flux of PAN0.5 might also be supported by slightly larger or more interconnected surface pores in combination with increased hydrophilicity. The MWCO value of all the membranes is around 50 kg/mol or lower, as the retention of a dextran with the molecular weight of 50 Kg/mol was approximately 90%.

3.6 Membrane compaction study

Compaction studies were conducted to observe the response of the porous structure of the membranes at increased pressures and its impact on water flux during the filtration. The flux of a component *i*, J_i, across a membrane often is a linear function of the transmembrane pressure (pressure drop) ΔP: [30]

$$J_i = L_i \cdot \Delta P \qquad (4)$$

L_i denotes the permeability coefficient of component *i* (permeance). Porous composite membranes may experience a reduction in flux under the effect of high pressure and this phenomenon can also be observed in the here studied PAN membranes. The majority of composite membranes can undergo compaction during the filtration process. This reduces the pore sizes or free volume inside the membrane and thus reduces the permeability coefficient, which leads to a reduction of permeate flux. Machado *et al.* [30] reported the dropping behaviour of flux with the

increase in transmembrane pressure for nanofiltration membranes, which can be expressed by equation 5, where $L°_i$ is the permeance under atmospheric pressure, and α is the compaction factor, respectively:

$$J_i = L_i° \cdot e^{-\alpha \cdot \Delta P} \cdot \Delta P \quad (5)$$

By comparing equations 4 and 5 the transmembrane pressure dependence of the permeability coefficient is obtained:

$$L_i = L_i° \cdot e^{-\alpha \cdot \Delta P} \quad (6)$$

For compaction studies, water was permeated through the membranes for 40 minutes at a transmembrane pressure of 2 bar. After this treatment the water flux was measured at 2, 4, 6, 8 and 10 bar, where each pressure was maintained for 10 minutes prior to the flux measurement. Figure 10 shows the mean flux as a function of pressure. The membrane compaction factor (α) can be calculated by plotting ln($J/\Delta P$) against the applied pressure drop ΔP (as shown in Figure 11), α being the slope of the straight line. The values of α are summarized in Table 2, where α for PAN2 was 36% lower compared to PAN0. Returning from 10 to 2 bar, the flux never came back to its initial value. The flux reduction can be calculated from water flux values measured at 2 bar before and after the pressure treatment. For PAN2, the flux reduction after pressure treatment was less compared to neat, PAN0.5 and PAN1 which shows that higher pressure application could be well sustained by PAN2 (Figure 12). After the flux measurements, the membranes were placed into a mixture of water and isopropanol (1:1) for 10 minutes for the pore opening. The water flux was recovered again which indicates the reversible nature of compaction.

3.7 Mechanical characterization

The tensile strength of PAN nanocomposite membranes as a function of MWCNTs content is shown in Figure 13. The tensile strength at break increases with MWCNTs addition. For PAN2 membranes it increased over 97% compared to PAN0 membranes. The increase in tensile strength of PAN nanocomposite membranes is expected as it is also well-known from fibre reinforced polymer composites, where the fillers are sufficiently bound to the matrix, i.e. have some good interactions (here: CH-π interactions as concluded from the Raman spectra shown in Figure 3). As in the present case porous materials are investigated, another reason is the decreased porosity of the nanocomposite membranes with increased filler loadings (Table 2). The similar effect is reported in literature where decrease in porosity of the PAN membranes was observed by increase in polymer solution concentration. Consequentally, membranes with less porosity showed good mechanical strength compared to highly porous membranes.[31]

4. Conclusions

PAN ultrafiltration nanocomposite membranes with improved properties were successfully prepared by a phase inversion process. The addition of MWCNTs led to the increase in polymer solution viscosity which indicates a good dispersion of the MWCNTs. The good dispersion was also confirmed by TEM. An indication for a good interaction between MWCNT and PAN was given by Raman spectroscopy. The increased solution viscosity suppressed the formation of macrovoids and led to a reduced number of bigger sized macrovoids compared to pure PAN membranes. However, the surface pore sizes seemed not affected by the viscosity of the composite solution, which was also reflected by the similar molecular weight cut off observed for all membranes under study (dextrane with a molecular weight of 50 Kg/mol was retained by approximately 90% on the feed side). Introduction of

MWCNTs enhanced the water flux of the membranes especially at 0.5 wt% loading. The water flux was reduced for membranes with higher loadings of MWCNTs, but it was still higher compared to pure PAN membranes in all cases. Moreover, the compaction of the membranes was significantly reduced upon larger pressures due to the reinforcement properties of the MWCNTs. Therefore, by addition of well-dispersed MWCNTs the transport properties of PAN membranes could be improved. Also the tensile strength of PAN nanocomposite membranes was improved with the addition of MWCNTs. The increase in tensile strength and resistance against compaction may result from the decrease in porosity and good interaction of MWCNTs with PAN. Hence, MWCNTs provide a way to improve the mechanical stability and transport properties of the PAN ultrafiltration membranes and enables their applications at high transmembrane pressures.

Acknowledgements

The authors want to acknowledge Clarissa Abetz for carrying out TEM investigations and analysing the results, Karen-Marita Prause for SEM, Heinrich Böttcher for mechanical characterisation, and Prof. Christine Jérôme, Dr. Michaël Alexendre (ULg, Belgium) and Petra Merten for helpful discussions. Sascha Crizeli from FutureCarbon is acknowledged for the MWCNTs used in this study. The work was financially supported by project “High Aspect Ratio Carbon-based Nanocomposites” (HARCANA) within the European Community's 7th Framework Programme for Research and Technological Development under the Grant Agreement number NMP3-LA-2008-213277.

References

[1] A. F. Ismail, P.S. Goh, S.M Sanip, M. Aziz, Transport and separation properties of carbon nanotube-mixed matrix membrane, Separation and Purification Technology 70 (2009) 12–26.

[2] M. Mulder, Basic Principles of Membrane Technology, 2nd Edition, Kluwer Academic Publisher, The Netherlands, 1996.

[3] K. Ebert, D. Fritsch, J. Koll, C. Tjahjawiguna, Influence of inorganic fillers on the compaction behaviour of porous polymer based membranes, J. membr. Sci. 233 (2004) 71-78.

[4] V.R. Tarnawski, P. Jelen, Estimation of compaction and fouling effects during membrane processing of cottage cheese whey, J. Food Eng. 5 (1986) 75-90.

[5] K.M. Persson, V. Gekas, G. Trägårdh, Study of membrane compaction and its influence on ultrafiltration water permeability, J. Membr. Sci. 100 (1995) 155-162.

[6] L. Yan, S. Hong, M. L. Li, Y. S. Li, Application of the Al2O3–PVDF nanocomposite tubular ultrafiltration (UF) membrane for oily wastewater treatment and its antifouling research, Separation and Purification Technology 66 (2009) 347–352.

[7] D. S. Kim, H. B. Park, Y. M. Lee, Y. H. Park, J. W. Rhim, Preparation and characterization of PVDF/Silica hybrid membranes containing sulfonic acid groups, J. App. Polymer Sci., 93 (2004) 209–218.

[8] C. Tang, Q. Zhang, K. Wang, Q. Fu, C. Zhang, Water transport behaviour of chitosan porous membranes containing multi-walled carbon nanotubes (MWNTs), J. Membr. Sci. 337 (2009) 240-247.

[9] E. Celik, H. Park, H. Choi, H. Choi, Carbon nanotube blended polyethersulfone membranes for fouling control in water treatment, Water Research 45 (2011) 274-282.

[10] L. Dumee, L. Velleman, K. Sears, M. Hill, J. Schutz, N. Finn, M. Duke, S. Gray, Control of porosity and pore size of metal reinforced carbon nanotube membranes, Membranes 1 (2011) 25-36.

[11] L. F. Dumée, K. Sears, J. Schütz, N. Finn. C. Huynh, S. Hawkins, M. Duke, S. Gray, Characterization and evaluation of carbon nanotube bucky-paper membranes for direct contact membrane distillation, J. Membr. Sci. 351 (2010) 36-43.

[12] J. H Choi, J. Jegal, W. N. Kim, H. S. Choi, Incorporation of multiwalled carbon nanotubes into poly(vinyl alcohol) membranes for use in the pervaporation of water/ethanol mixtures, J. App. Polym. Sci., 111 (2009) 2186-2193.

[13] X. Peng, J. jin, Y. Nakamura, T. Ohno, I. Ichinose, Ultrafast permeation of water through protein-based membranes, Nature Technology 4 (2009) 353-357.

[14] A. I. Skoulidas, D. M. Ackerman, J. K. Johnson,D. S. Sholl, Rapid transport of gases in carbon nanotubes, Phy. Rev. Letters 89 (2002) 185901-1-4.

[15] S. Joseph, N. R. Aluru, Why are carbon nanotubes fast transporters of water, Nano Letters 8 (2008) 452-458.

[16] M. Majumder, N. Chopra, R. Andrews, B. J. Hinds, Enhanced flow in carbon nanotubes, Nature 438 (2005) 44.

[17] B. J. Hinds, N. Chopra, T. Rantell, R. Andrews, V. Gavalas, L. G. Bachas, Aligned MWCNTs membranes, Science 303 (2004) 62-65.

[18] M. Majumdar, N. Chopra, B. J. Hinds, Effect of tip functionalization on transport through vertically oriented carbon nanotube membranes, J. Am. Chem. Soc. 127 (2005) 9062-9070.

[19] S. Kim, J. R. Jinschek, H. Chen, D. S. Scholl, E. Marand, Scalable fabrication of carbon nanotube/polymer nanocomposite membranes for high flux gas transport, Nano Letters 7 (2007) 2806-2811.

[20] S. Kim, T. W. Pechar, E. Marand, Poly(imide siloxane) and carbon nanotube mixed matrix membranes for gas separation, Desalination 192 (2006) 330-339.

[21] J. H. Choi, J. Jegal, W. N. Kim, Fabrication and characterization of multi-walled carbon nanotubes/polymer blend membranes, J. Membr. Sci. 284 (2006) 406-415.

[22] H. R. Lohokare, S. C. Kumbharkar, Y. S. Bhole, U. K. Kharul, Surface Modification of Polyacrylonitrile Based Ultrafiltration Membrane, J. Applied Polym. Sci., 101, (2006), 4378-4385.

[23] Z. Q. Huang, Z. Y. Chen, X. P. Guo, Z. Zhang, C. L. Guo, Structures and separation properties of PAN-Fe3O4 ultrafiltration membranes prepared under an orthogonal magnetic field, Ind. Eng. Chem. Res. 45 (2006) 7905-7912.

[24] O. Marie, F. T. Starzyk, J. C. Lavalley, Confirmation of strongest nitrile-hydroxy groups interaction in the side pockets of mordenite zeolites, Phys. Chem. Chem. Phys. 2 (2000) 5341-5349.

[25] D. Baskaran, J. W. Mays, M. S. Bratcher, Noncovalent and Nonspecific Molecular Interactions of Polymers with Multiwalled Carbon Nanotubes, Chem. Mater. 17, (2005), 3389-3397.

[26] Y. Y. Huang, S. V. Ahir, and E. M. Terentjev, Dispersion rheology of carbon nanotubes in a polymer matrix, Physical Review B 73 (2006) 125422.

[27] B. B. Khatua, D. J. Lee, H. Y. Kim, J. K. kim, Effect of organoclay platelets on morphology of nylon-6 and poly(ethylene-ran-propylene) rubber blends, Macromolecules, 37 (2004) 2454-2459.

[28] S. Qiu, L. Wu, X. Pan, L. Zhang, H. Chen, C. Gao, Preparation and properties of functionalized carbonnanotube/PSF blend ultrafiltration membranes, J. Membr. Sci. 342 (2009) 165-172.

[29] N. Stafie, D.F. Stamatialis, M. Wessling, Insight into the transport of hexane–solute systems through tailor-made composite membranes, J. Membr. Sci. 228 (2004) 103-116.

[30] D. R. Machado, D. Hasson, R. Semiat, Effect of solvent properties on permeate flow through nanofiltration membranes. Part I: investigation of parameters affecting solvent flux, J. Membr. Sci. 163 (1999) 93–102.

[31] N. Scharnagl, H. Buschatz, Polyacrylonitrile (PAN) membranes for ultra- and microfiltration, Desalination 139(2001) 191-198.

6. Figures

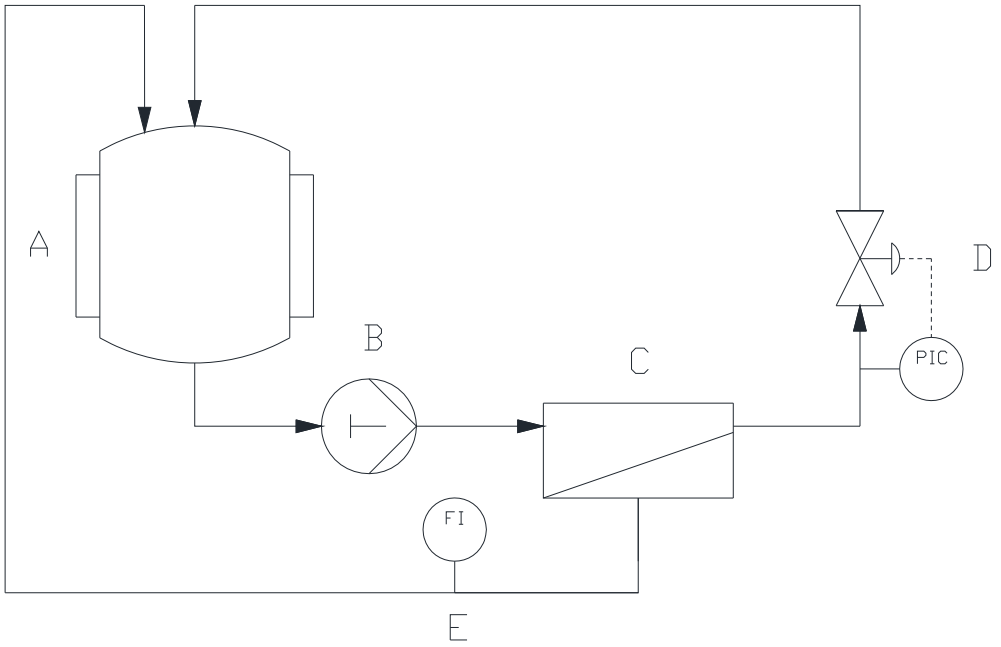

Figure 1: Schematic diagram of cross flow mode depicting different parts: (A) Support vessel, (B) Feed pump, (C) Membrane cell, (D) PIC (Pressure indicator and controller), (E) FI (Flow indicator).

.

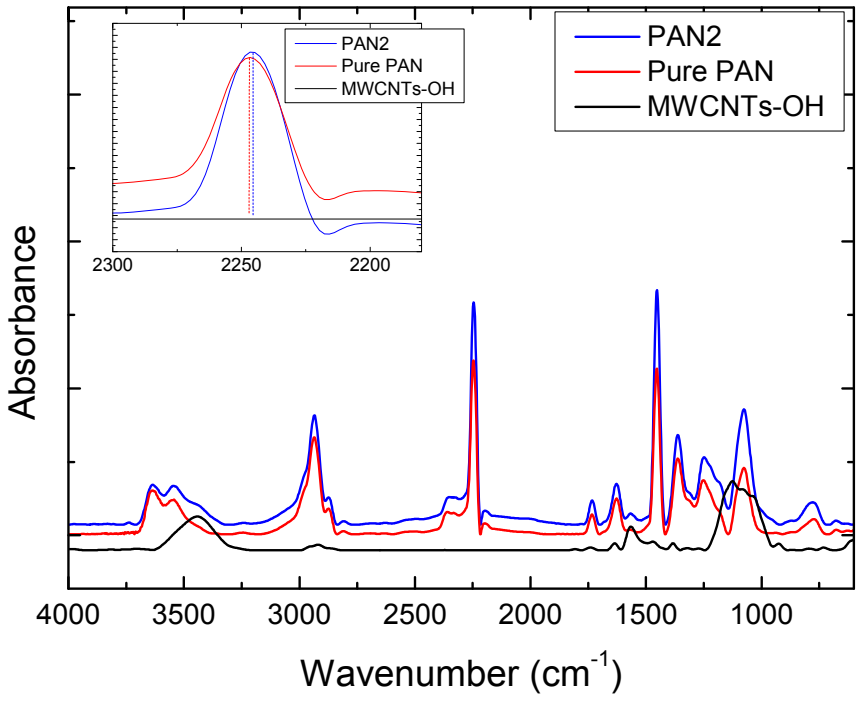

Figure 2: FTIR spectra of MWCNTs and PAN nanocomosite membranes.

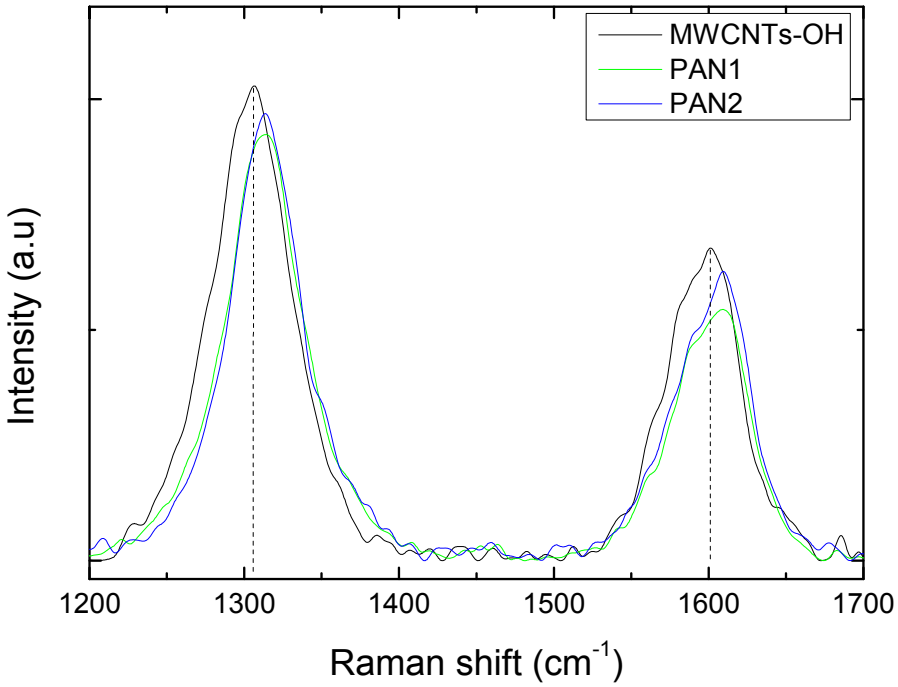

Figure 3: Raman spectra of MWCNTs, PAN1 and PAN2.

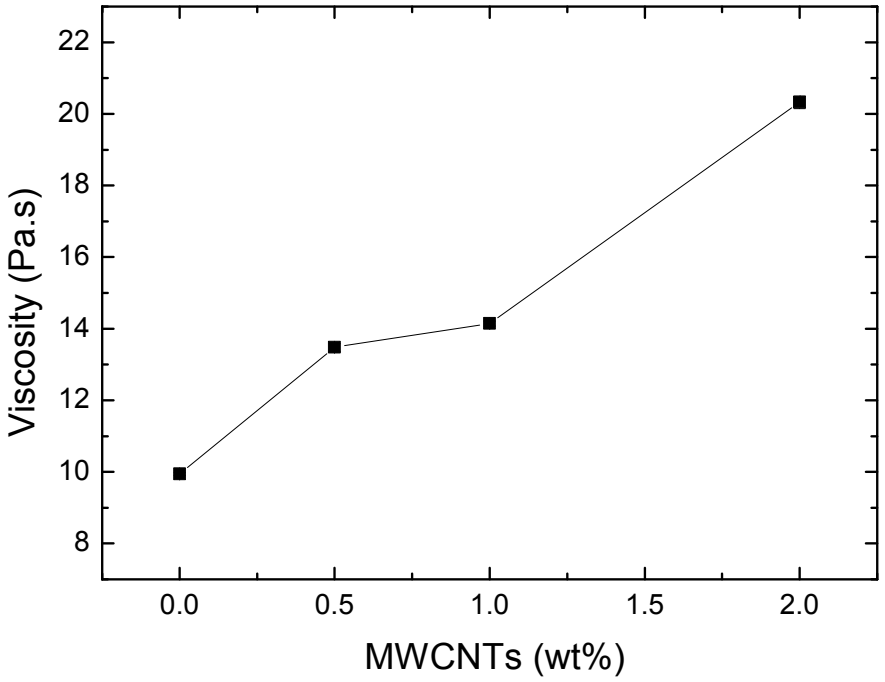

Figure 4: Viscosity of PAN solutions with different MWCNTs loading

(a)

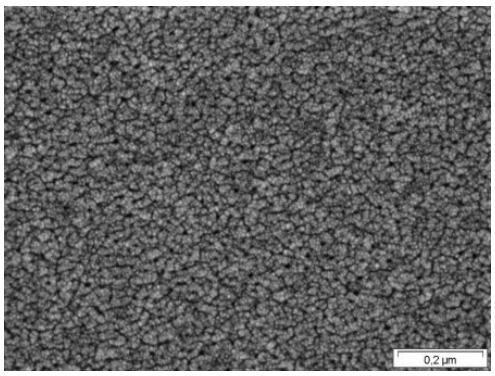

(b)

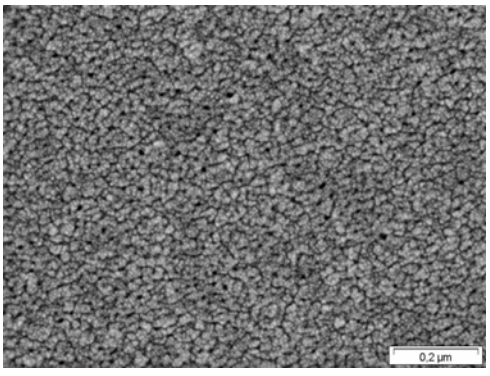

(c) (d)

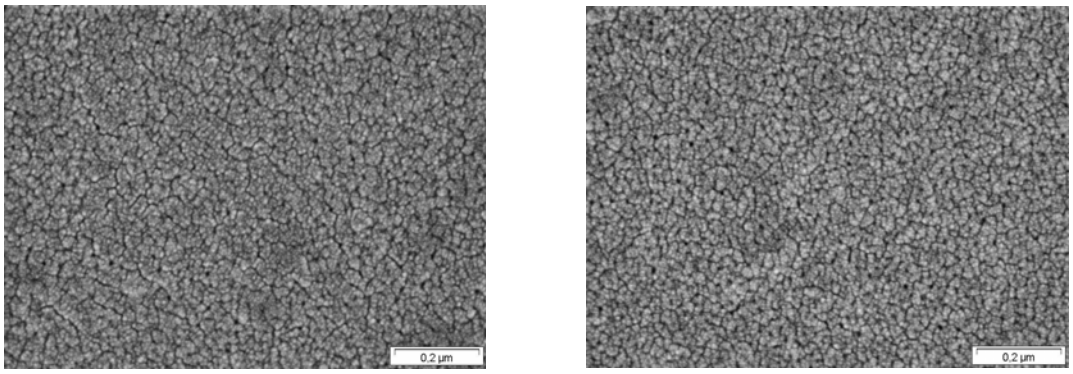

Figure 5: SEM surface images of PAN membranes (a) PAN0, (b) PAN0.5, (c) PAN1 and (d) PAN2 (scale bar for a to d is 200 nm)

(a) (b)

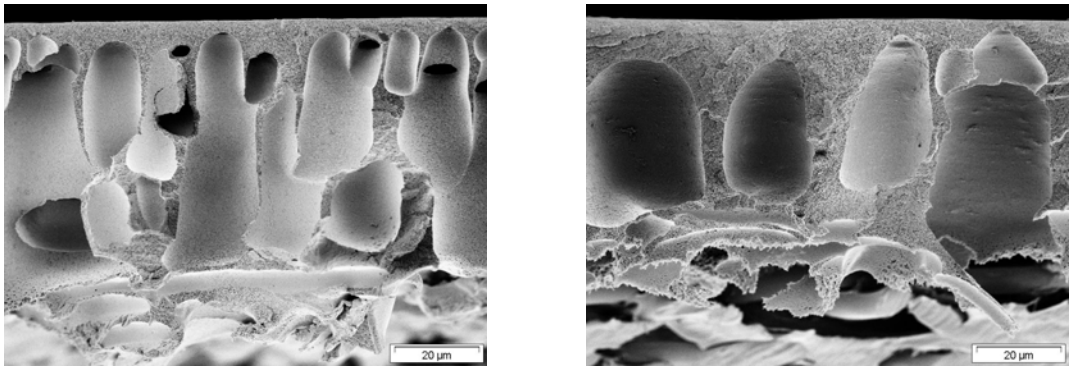

(c) (d)

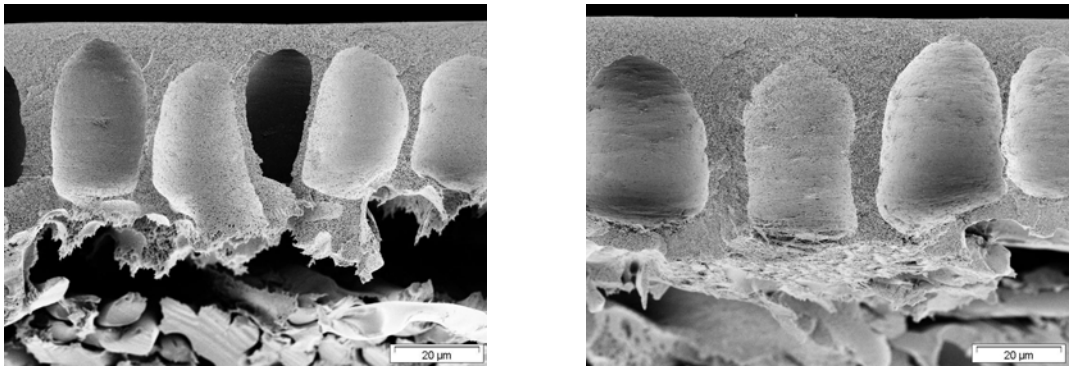

(e)

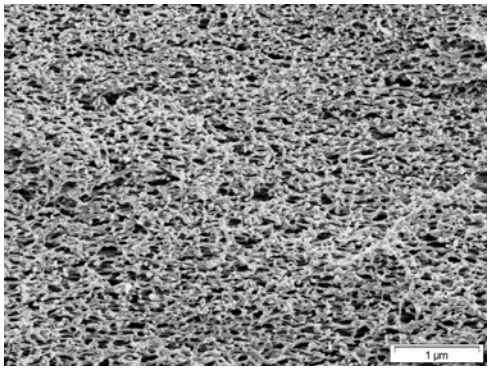

Figure 6: SEM cross-section images of PAN membranes (a) PAN0, (b) PAN0.5, (c) PAN1, (d) PAN2 and (e) magnified PAN2. Scale bar for images a to d is 20µm, and for e it is 1µm.

(a) (b)

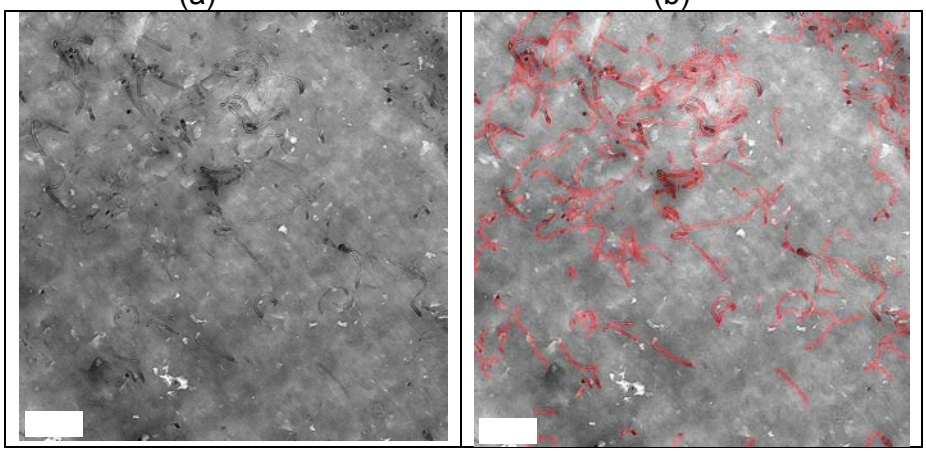

Figure 7: TEM image of PAN nanocomposite membranes loaded with 2wt% MWCNTs (a) Original TEM image (b) manipulated TEM image to highlight MWCNTs (red) (scale bar 200 nm)

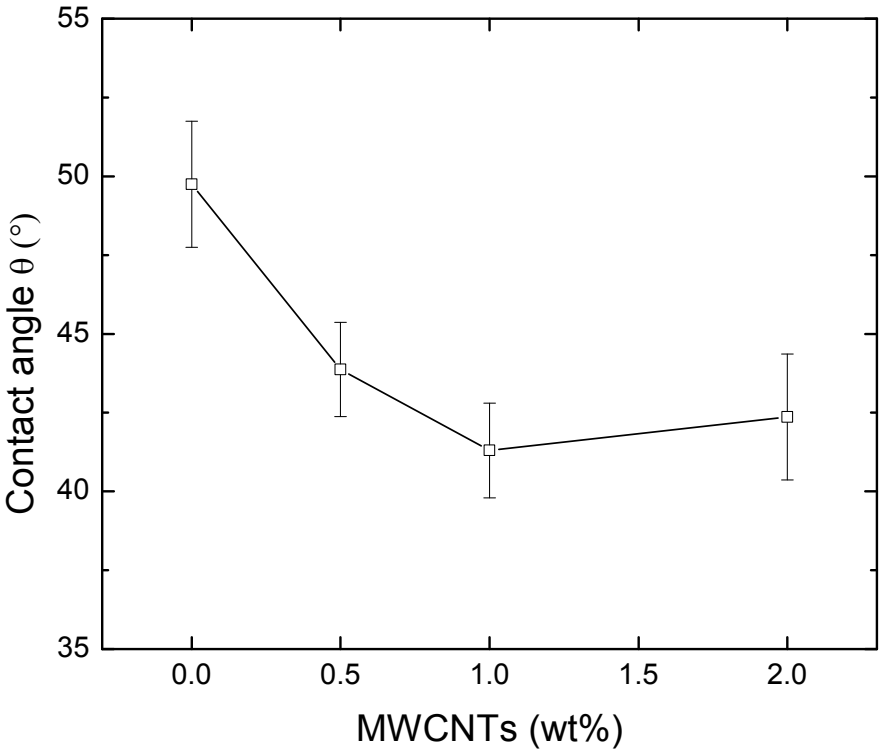

Figure 8: Surface contact angles of PAN nanocomposite membrane as a function of MWCNTs loading.

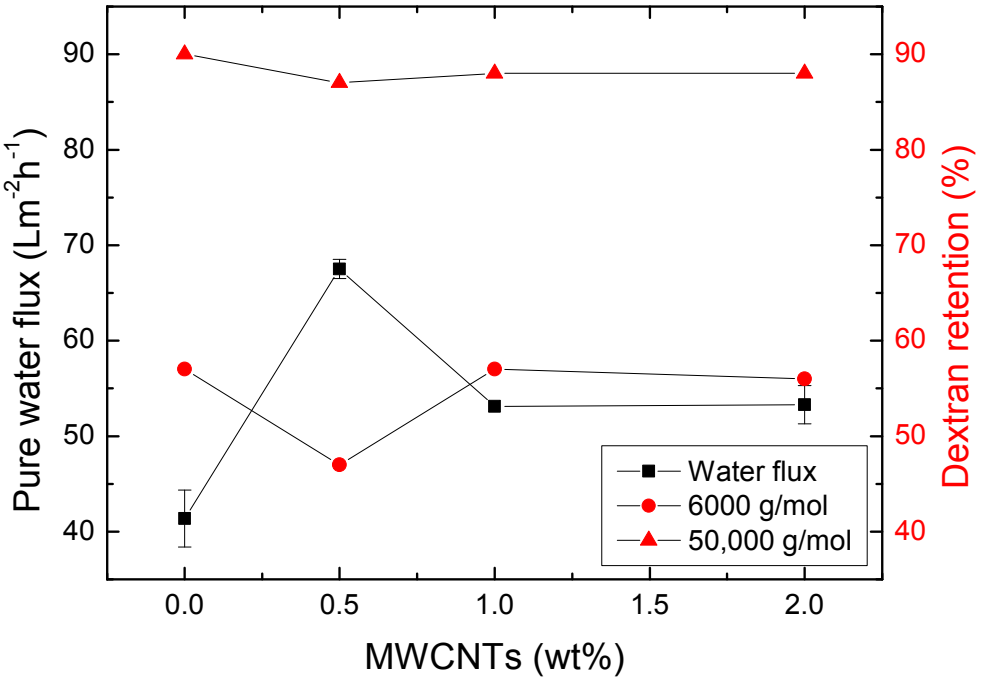

Figure 9: Water flux (left) and retention of 330 ppm solution of dextrans (right) of PAN nanocomposite membrane with different loading of MWCNTs.

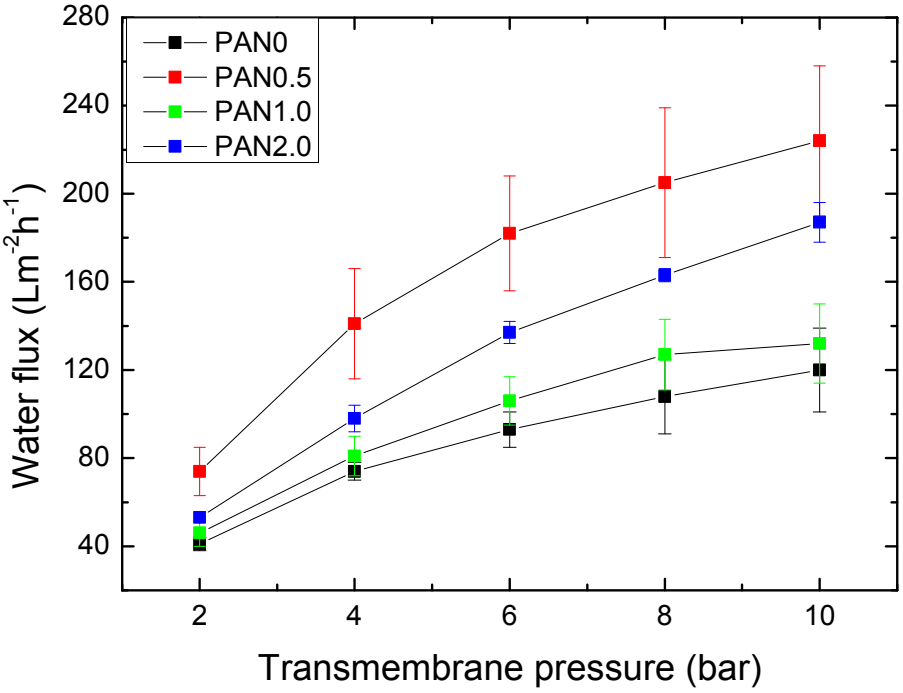

Figure 10: Water flux of PAN nanocomposite membranes as function of transmembrane pressure ΔP.

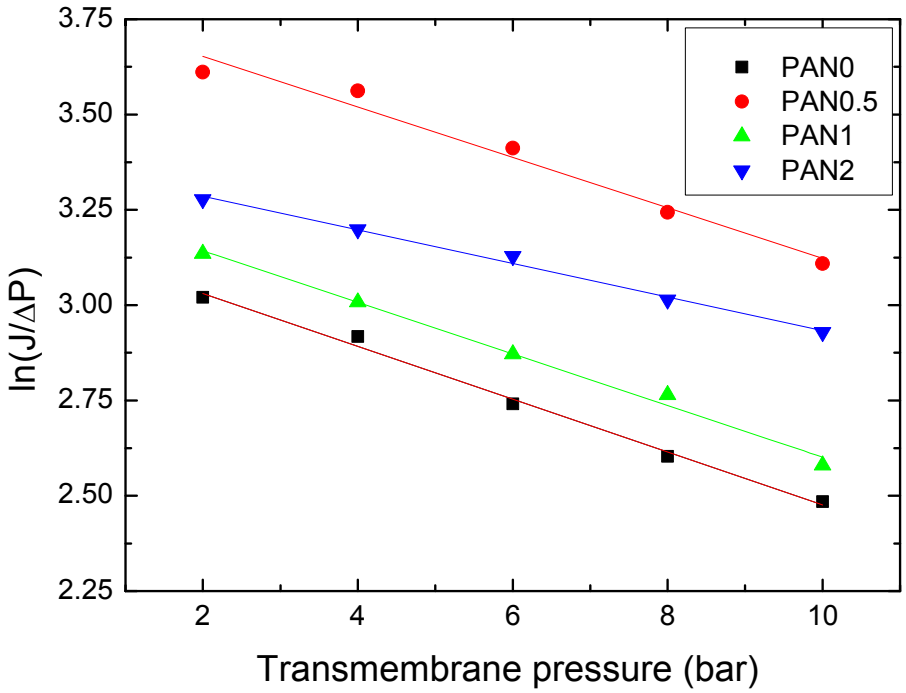

Figure 11: Plot of the ln(J/ΔP) as a function of the transmembrane pressure ΔP for compaction characterization.

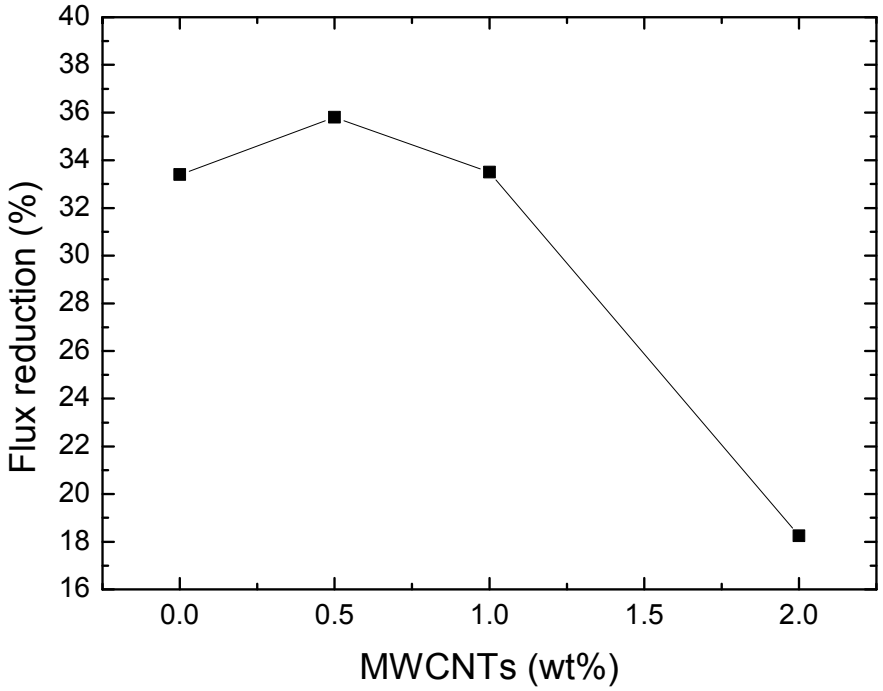

Figure 12: Water flux reduction before and after the variation of the transmembrane pressures from 2 to 10 bar as a function of MWCNTs content.

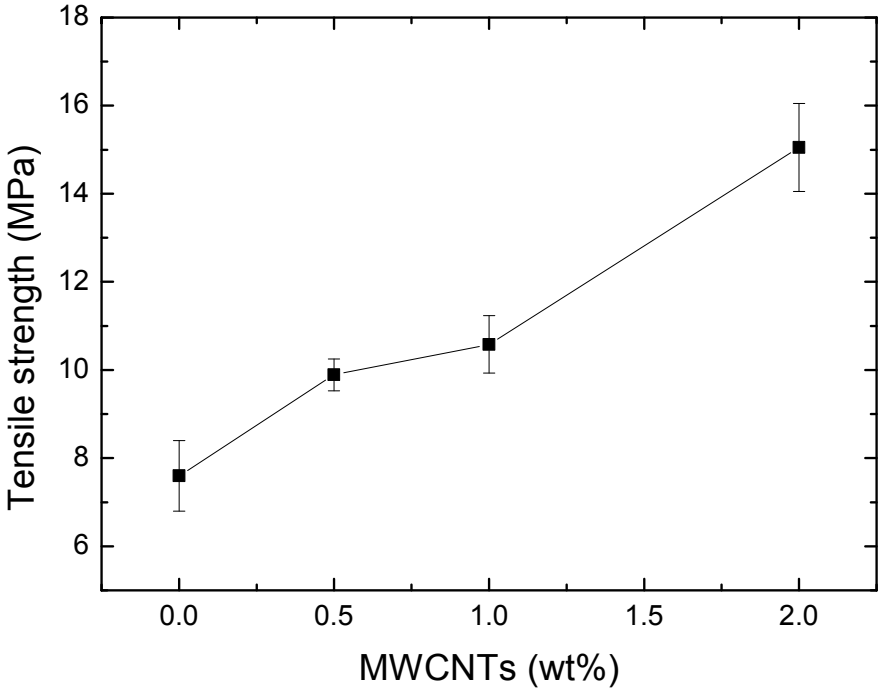

Figure 13: Tensile strength at break as a function of MWCNTs loading (wt%)

Table 1: Data of molecular weight of dextrans used for retention measurements

Dextran Type	Molecular weight (g/mol)
Dextran FP1	900-1200
Dextran 4	4000-6000
Dextran 35	35,000-50,000
Dextran 100	100,000-200,000
Dextran 500	350,000-550,000

Table 2: Data of the membrane structure

Membrane	**Pore Size (nm)***	**Porosity (%)**	**Compaction factor (α) bar^{-1}**
PAN0	11 (±3)	67	0.069
PAN0.5	11 (±2)	59	0.066
PAN1	11 (±2)	57	0.067
PAN2	10 (±2)	47	0.044

* Calculated by SEM